Crystallization behavior of phase change nanostructures

Simone Raoux[1a], Charles T. Rettner[1], Jean L. Jordan-Sweet[2], Martin Salinga[1,3], and Michael F. Toney[4]

[1]IBM Macronix Infineon PCRAM Joint Project, IBM Almaden Research Center, 650 Harry Road, San Jose, California 95120
[2]IBM Macronix Infineon PCRAM Joint Project, IBM T. J. Watson Research Center, Yorktown Heights, New York 10598
[3]1. Physikalisches Institut 1A der RWTH Aachen, 52056 Aachen, Germany
[4]Stanford Synchrotron Radiation Laboratory, Stanford, CA 94025

ABSTRACT

Electron beam lithography was used to fabricate large hexagonal arrays of nanopillars of both $Ge_{15}Sb_{85}$ and $Ge_2Sb_2Te_5$. These nanostructures had a 65 nm diameter on a pitch of 100 nm. A low temperature lithographic process was used to keep the nanostructures in the amorphous state during patterning. Using time-resolved X-ray diffraction, the crystallization behavior of the nanostructures was studied and compared to blanket films. It was found that the amorphous to fcc phase transition occurs at the same temperature (150ºC for a heating rate of 1 ºC/s) for the blanket $Ge_2Sb_2Te_5$ film and the nanopatterns. The fcc to hexagonal phase transition that occurs for the blanket film at 360ºC is not observed for the nanostructures in the measured temperature range. For the $Ge_{15}Sb_{85}$ nanopatterns and blanket film the amorphous to crystalline phase transition occurred also at the same temperature (260ºC). The fact that the patterns and blanket film crystallize at the same temperature is an encouraging result for the scalability of phase change solid state memory devices.

Keywords: Crystallization, phase transition, scaling, nanostructures, XRD

1. INTRODUCTION

A novel class of solid state storage devices based on phase change materials has been reported in the literature[1-5]. These devices rely on the change in resistivity that accompanies the change in phase that occurs during switching between the crystalline, low resistivity phase and the amorphous, high resistivity phase. The devices are switched from the amorphous to the crystalline state by applying a current pulse that is high and long enough to heat the phase change material over its crystallization temperature and crystallize it. Switching back to the amorphous state is performed by applying a larger current pulse with a short fall time that heats the phase change material (or fractions of it) over its melting point and fast quenching prevents the material from re-crystallizing. The devices have been typically fabricated in pore structures based on 0.18 μm, 0.12 μm or 0.1 μm CMOS technology[1-4] with contact diameters to the phase change material as small as 50nm. Another implementation describes planar structures with phase change wires having cross-sections as small as 225 nm[2,5]. Scaling of phase change memory devices is generally favorable since smaller devices or contact areas lead to a reduction in the currents that are required to switch the devices. The most common phase change material found in solid state devices is $Ge_2Sb_2Te_5$ (GST) without[1,2,4] or with doping with various elements such as nitrogen[3], tin[6], and silicon[7]. Other materials such as doped SbTe[5] have also been applied in devices.
Most material properties such as crystallization behavior and resistivity as a function of temperature have been studied on blanket films. However, it is known that many material parameters can deviate from the bulk value for nanostructures, for example as the melting point varies with particle size for Au nanoparticles[8]. In the present paper we describe x-ray diffraction (XRD) experiments directed towards the study of scaling behavior of phase change nanoparticles.

2. EXPERIMENTAL

Nanostructures were fabricated from GST and $Ge_{15}Sb_{85}$ (GeSb), another phase change material that is widely described in the literature[9,10] and that is of particular interest because of its long archival life. The nanostructures were fabricated using electron beam lithography from 50nm thick films deposited on 1 μm-thick SiO_2 on Si substrates and capped with 5nm Ta. The GST was sputter-deposited from a stoichiometric compound target, and GeSb was deposited by co-sputtering from a Ge

[a]Please send correspondence to simone_raoux@almaden.ibm.com

and an Sb source. The patterns were made by ebeam lithography using 950k PMMA resist. In order to minimize any annealing of the samples, the resist was only baked to 105°C, which is just above the glass transition temperature of the PMMA.
The nanostructures extended over an area of 2mmx5mm that was larger than the x-ray probe beam. Figs. 1 and 2 show SEM images of the nanostructures. The diameter of the nanostructures was about 65nm on a 100nm pitch. An hexagonal array was chosen in order to achieve maximum packing density and maximum x-ray diffraction signal. It is apparent that the nanostructures are well defined over a large area and well separated.

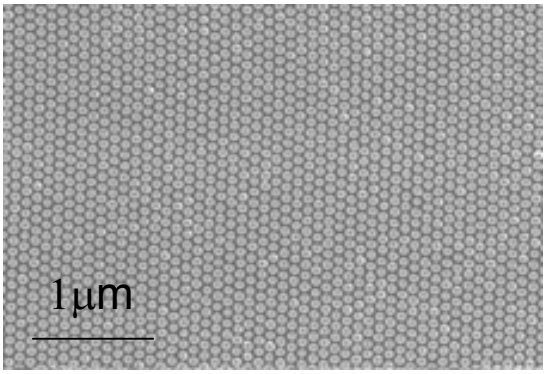

Fig. 1: SEM image of GST nanostructures

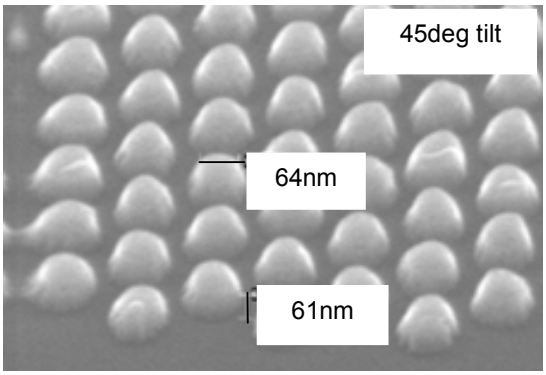

Fig. 2: SEM image of GST nanostructures

Time-resolved *in-situ* x-ray diffraction (XRD) was employed to study the structural properties of blanket films and the nanostructures. These experiments were performed at beamline X-20C of the National Synchrotron Light Source using a photon energy of 6.9 keV. The set-up consisted of a high-throughput synthetic multilayer monochromator and fast linear-diode-array detector[11,12]. A special chamber for controlling the sample ambient (purified He gas) was outfitted with a BN heater for rapid annealing up to 1200ºC at a rate of ≤ 35ºC/sec.[13,14] Grazing-incidence x-ray diffraction measurements were made at beamline X20A at the National Synchrotron Light Source on the blanket films and nanostructures after heating to 450C in the time-resolved XRD set-up at a rate of 1ºC/sec. The x-ray energy was 8.047 keV and the diffractometer was configured for high resolution using a single-bounce Ge(111) analyzer crystal upstream of the detector. The instrumental resolution was determined by scanning the incident beam with the detector arm, resulting in a full width at half maximum (FWHM) of 0.0008 in units of the scattering vector q, where $q = (4\pi\sin\theta)/\lambda$ (θ is the diffraction angle and λ the wavelength). Radial scans (*h*-scans) were taken at a fixed incidence angle of 0.49 degrees. The angles of incidence α and reflection β at the sample surface were constrained to be equal and constant throughout the radial scans. The grazing incidence geometry minimizes contributions from the substrate and measures diffraction planes perpendicular to the surface. In thin film samples, this eliminates broadening due to the finite film thickness.

3. RESULTS

Blanket films and nanostructures of GST and GeSb were heated in the *in-situ* XRD set-up at a rate of 1ºC/sec and the diffracted peak intensity was recorded with the linear detector over a 2θ range of 24-40 degrees. This angular range contains strong diffraction peaks for both, the GST and GeSb. Figure 3 shows the diffraction peak intensities during annealing for GST blanket film and nanopatterns, and Fig. 4 shows results for GeSb.
For the GST blanket film we observe a transition from the amorphous phase to the metastable fcc phase at a temperature of 150ºC, and a transition from the fcc phase to the stable hexagonal phase at a temperature of about 360ºC. This agrees very well with literature data[15]. For the nanopatterns we observe that the amorphous to fcc phase transition occurs at the same temperature as for the blanket film. The fcc to hexagonal phase transition does not occur within the temperature range up to 450ºC. We had found previously on larger nanopatterns between 100 μm and 100nm particle diameter that the amorphous-fcc phase transition occurs at the same temperature for nanopatterns and blanket films, but that the fcc-hexagonal phase transition is shifted to higher temperatures for the smallest nanopatterns. The fact that the hexagonal phase is not formed might actually be an advantage for memory device applications since the fcc phase has a higher resistivity than the hexagonal phase[15] and needs a lower current to provide the power to melt the material for the *reset* operation.

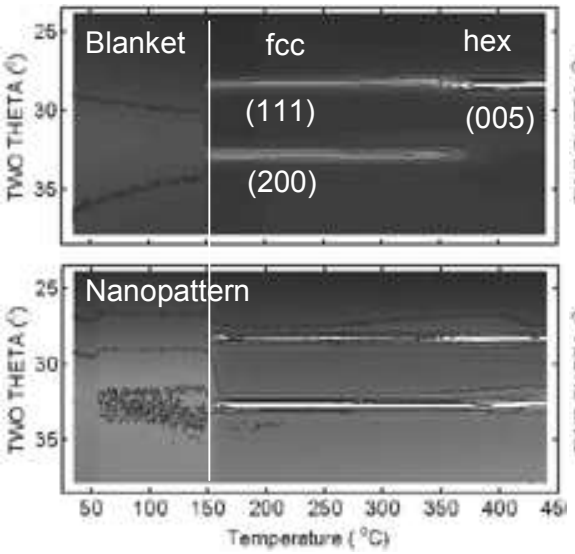

Fig. 3: Intensity of XRD peaks as a function of temperature for GST

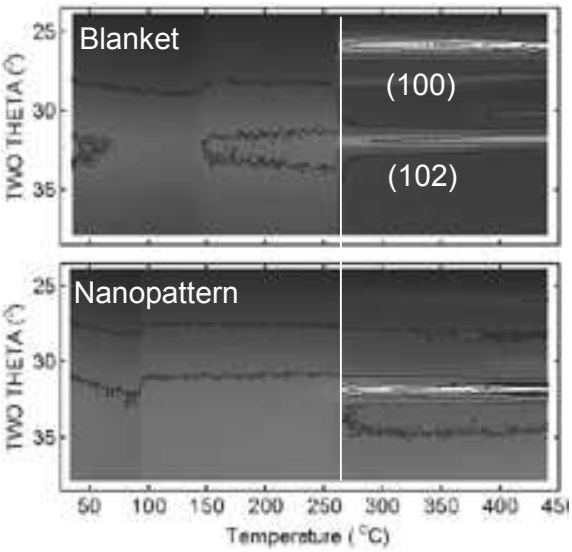

Fig. 4: Intensity of XRD peaks as a function of temperature for GeSb

For the GeSb material we find also that the amorphous-to-crystalline phase transition occurs at the same temperature of 260ºC for blanket films and nanopatterns. This also agrees with literature where a crystallization temperature of 250ºC was reported for $Ge_{15}Sb_{85}$.[10] The crystallographic texture differs between nanopatterns and blanket films for both GST and GeSb.

In order to evaluate the effect of the patterning on the grain size we performed grazing incidence XRD experiments. Figure 5 shows the grazing-incidence XRD spectra for GST and GeSb. In particular, for the GST samples the clearly visible broadening of the peaks in the nanopatterned sample compared to the blanket film is indicative of a grain size reduction. The grain size was estimated from the peak widths using the Scherrer formula ($t=0.9\lambda/B\cos\Theta_B$)[16] that calculates the grain diameter t from the FWHM of the diffraction peak intensity B for a peak centered at the angle Θ_B.

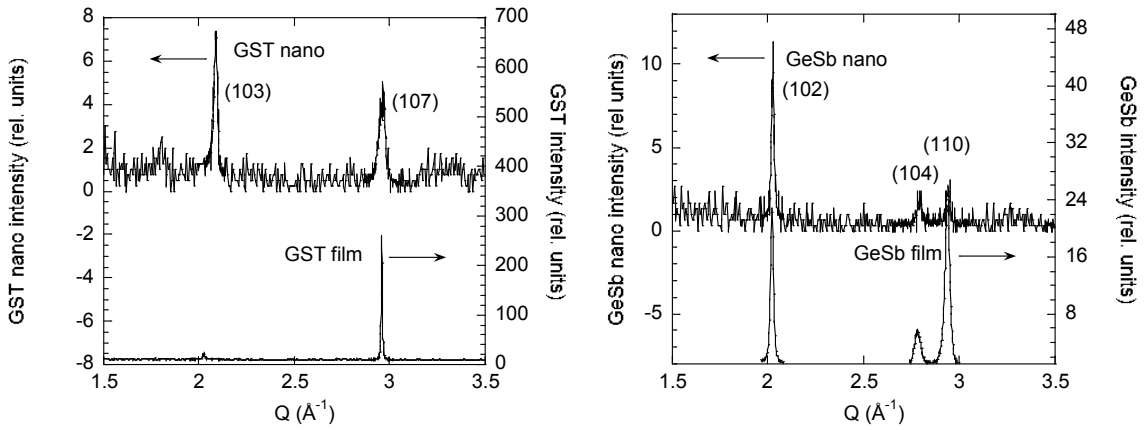

Fig. 5: Grazing incidence XRD spectra for GST (left) and GeSb (right) blanket films and nanopatterns. The spectra are offset for clarity.

The grain size obtained from the Scherrer formula depends upon the actual diffraction peak that is used for the analysis, since different broadening mechanisms contribute to the peak width for different peaks. We estimated most probable grain diameters of 40-140 nm for blanket GST and 20-30nm for GST nanostructures. The reduction in grain size is not surprising since the largest grains for the blanket film are larger than the nanopatterns. The nanopatterns seem to consist of only a few grains. For the GeSb material the estimated grains are similar for the blanket film and the nanopatterns, between 15 and 35 nm.

In a more detailed analysis the diffraction spectra were fitted by a simulation program that assumed different grain size distributions for the different peaks[17]. The most probable grain diameter determined by simulation was 25-45 nm for the GeSb blanket film and 20-25 nm for the GeSb nanostructures, and 30-80 nm for the GST blanket films. We were not able to fit satisfactorily the data for the GST nanostructures due to a high noise level in the data. This analysis showed a slight reduction in grain size due to patterning for the GeSb nanostructures compared to the blanket film.

SUMMARY

Nanostructures with 65 nm diameter and 100 nm pitch have been fabricated from $Ge_{15}Sb_{85}$ and $Ge_2Sb_2Te_5$ phase change materials over large areas. Time-resolved *in-situ* XRD measurements show that the nanostructures crystallize at the same temperature as blanket films of the same material. The fcc-hexagonal phase transition that was observed at 360ºC for blanket GST film does not occur in the nanostructures. It was also observed that nanopatterning leads to a reduction in grain size, particularly for the GST nanostructures. Both findings are encouraging for the study of scaling of phase change materials directed towards non-volatile memory storage devices. The crystallization behavior studied for blanket films can be extrapolated for nanostructures down to 65 nm size and data obtained on blanket films are useful for the research regarding devices. The reduction in grain size is also favorable since smaller grains typically lead to higher resistivity of the materials in the crystalline phase which in turn leads to a desirably smaller required current for switching the devices.

ACKNOWLEDGEMENTS

This research was carried out in part at The National Synchrotron Light Source, Brookhaven National Laboratory, which is supported by the U.S. Department of Energy, under Contract No. DE-AC02-98CH10886. Portions of this research were carried out at the Stanford Synchrotron Radiation Laboratory, a national user facility operated by Stanford University on behalf of the U.S. Department of Energy, Office of Basic Energy Sciences.

REFERENCES

1. A. Redaelli, A. Pirovano, F. Pellizer, A. L. Lacaita, D. Ielmini, and R. Bez, IEE Trans. Electr. Dev. Lett. **25**, 684 (2004)
2. A. Pirovano, A. Redaelli, F. Pellizzer, F. Ottogalli, M. Tosi, D. Ielmini, A. L. Lacaita, and R. Bez, IEEE Tans. Dev. Mat. Reliability **4**, 422 (2004)
3. S. J. Ahn, Y. N. Hwang, Y. J. Song, S. H. Lee, S. Y. Lee, J. H. Park, C. W. Jeong, K. C. Ryoo, J. M. Shin, J. H. Park, Y. Fai, J. H. Oh, G. D. Koh, G. T. Jeong, S. H. Joo, S. H. Choi, Y. H. Son, J. C. Shin, Y. T. Kim, H. S. Jeong, and Kinam Kim, *2005 Symp. VLSI Technology Dig. Techn. Papers,* p. 98
4. S. L. Cho, J. H. Yi, Y. H. Ha, B. J. Kuh, C. M. Lee, J. H. Park, S. D. Nam, H. Horii, K. C. Ryoo, S. O. Park, H. S. Kim, U-In. Chung, J. T. Moon, and B. I Ryu, *2005 Symp. VLSI Technology Dig. Techn. Papers,* p. 96
5. M. Lankhorts, B. S. M. M. Ketelaars, and R. A. M. Wolters, Nature Mat. **4**, 347 (2005)
6. S. L. Cho, H. Hoorii, J. H. Park, J. H. Yi, B. J. Kuh, Y.H.Ha, S. O. Park, H. S. Kim, U. I. Chung, and J. T. Moon, *European Symp. Phase Change and Ovonic Sci.,* Balzers, Lichtenstein, 2004
7. Y. C. Chen, H. P. Chen, Y. Y. Liao, H. T. Lin, L. H. Chou, J. S . Kuo, P. H. Chen, S. L. Lung, and R. Liu, *2003 Int. Symp. VLSI Technology, Systems and Applications,* Proc. Techn. Papers, Hsinchu, Taiwan, p. 32
8. K. Dick, T. Dhanasekaran, Z. Zhang, and D. Meisel, J. Am. Chem. Soc. **124**, 2312 (2002)
9. L. van Pieterson, M. van Schijndel, J. C. N. Rijpers, and M. Kaiser, Appl. Phys. Lett. **83**, 1373 (2003)
10. L. van Pieterson, M. H. R. Lankhorst, A. E. T. Kuiper, and J. H. J. Roosen, J. Appl. Phys. **97**, 83520 (2005)
11. G. B. Stephenson, Nucl. Instrum. Meth. Phys. Res. A **266**, 447 (1988)

12. G. B. Stephenson, K. F. Ludwig, Jr., J. L. Jordan-Sweet, S. Brauer, J. Mainville, Y. S. Yang, and M. Sutton, Rev. Sci. Instrum. **60**, 1537 (1989)
13. L.A. Clevenger, R.A. Roy, C. Cabral, Jr., K.L. Saenger, S. Brauer, G. Morales, K.F. Ludwig, Jr., G. Gifford, J. Bucchignano, J. Jordan-Sweet, P. DeHaven, and G.B. Stephenson, J. Mater. Res. **10**, 2355 (1995)
14. C. Lavoie, C. Cabral, Jr., L.A. Clevenger, J.M.E. Harper, J. Jordan-Sweet, K.L. Saenger, and F. Doany, Mater. Res. Soc. Symp. Proc. **406**, 163 (1996).
15. I. Friedrich, V. Weidenhof, W. Njoroge, P. Franz, and M Wuttig, J. Appl. Phys. **87**, 4130 (2000)
16. B. D. Cullity, *Elements of X-Ray Diffraction*, Addison-Wesley Publishing Comp., 1978
17. W.L. Prater, E.L. Allen, W.-Y. Lee, M.F. Toney, A. Kellock, J.S. Daniels, J.A. Hedstrom, and T. Harrell, J. Appl. Phys. 97, 093301 (2005)